Complementary Absorption versus Morphology in All-Conjugated Block Copolymer Solar Cells

Hisham Idriss, Adèle Gapin, Wissem Khelifi, Sylvie Blanc, Iyad Karamé, Sylvain Chambon, Lionel Hirsch, Antoine Bousquet, Christine Lartigau-Dagron

Complementary Absorption versus Morphology in All-Conjugated Block Copolymers Solar Cells

Hisham Idriss[a], Adèle Gapin[a], Wissem Khelifi[a], Sylvie Blanc[a], Iyad Karamé[b], Sylvain Chambon[c,d], Lionel Hirsch[d], Antoine Bousquet*[a], Christine Lartigau-Dagron*[a]

[a] Université de Pau et des Pays de l'Adour, E2S UPPA, CNRS, IPREM, Pau, France

[b] Laboratory of Catalysis, Organometallic and Materials (LCOM), Department of Chemistry, Lebanese University, Faculty of Sciences I, Hariri campus, Hadath, Lebanon

[c] LIMMS/CNRS-IIS (UMI2820), Institute of Industrial Science, The University of Tokyo, 4-6-1 Komaba, Meguro-ku, Tokyo, 153-8505, Japan

[d] Univ. Bordeaux, IMS, CNRS, UMR 5218, Bordeaux INP, ENSCBP, F-33405 Talence, France

Graphical abstract

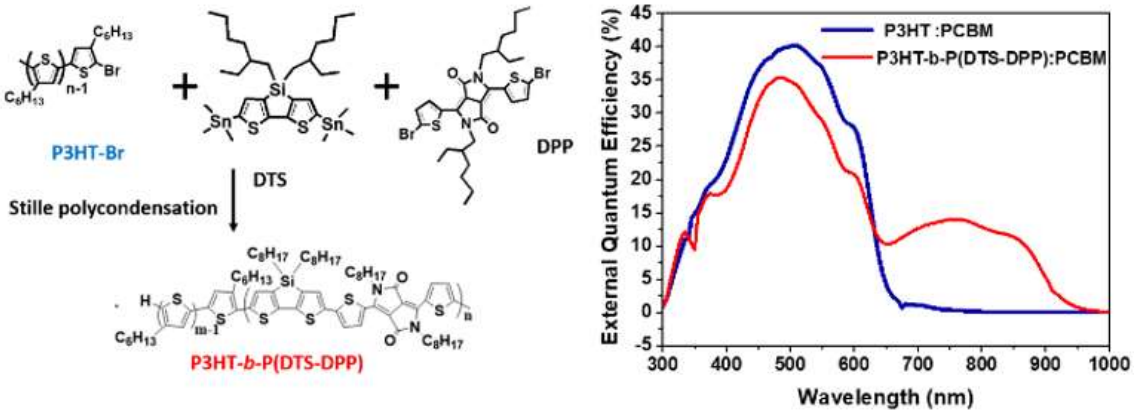

Abstract:

An efficient and simple method for synthesizing all-conjugated diblock copolymer is reported, using Stille polycondensation of A-A (dithienosilole) and B-B (diketopyrrolopyrrole) monomers with a macro end-capping agent P3HT. Diblock and triblock copolymers were produced with a molar composition that was tuned *via* the macromonomer molar mass and feed ratio. The molar mass and topology of the macromolecules obtained are discussed on the basis of the Carothers equation, conversion and monomer ratio. Spectrophotometry and cyclic voltammetry were used to highlight the complementarity of block absorption and the donor-acceptor nature of copolymers. Finally, integration in solar cells has been successfully performed with efficiencies reaching 2%. The performances of the devices were molar composition dependent and revealed that performance enhancement provided by the low band-gap block absorption was balanced by the copolymer nano-structuration that shrinks the charge collection at electrodes.

1. Introduction

In a world struggling to find enough energy to answer mankind demand, all renewable and carbon neutral sources must be considered and studied. Among them, sun could provide a nice solution if efficient solar cells with low environmental footprint are developed. Organic and polymer solar cells have received considerable attention the last decades because they provide complementary advantages compared to the silicon technology, such as light weight, flexibility, low cost and facile large-scale production.[1] The active layer of such devices is composed of a bulk heterojunction of two components: electron donor and acceptor. Most of the couples used are constituted by a π-conjugated polymer as electron donor and a fullerene derivative acceptor. Since the latter presents a negligible light absorption in the visible-near infrared regions, it has been recently replaced by "non-fullerene acceptor", often offering a useful complementary absorption in the 600-900 nm spectral region.[2]

Conjugated block copolymers (CBP) have also shown the potential to present complementary absorption in a single macromolecule. For example, several research teams have synthesized block copolymers made of poly(3-hexylthiophene) (P3HT) absorbing in the 400-550 nm range and different polymers absorbing at higher[3, 4] or lower[5, 6] wavelengths. Actually, diblock copolymers have the potential to bring more than complementary absorption because they can also be engineered to present in the same molecule an electron donor block coupled with an electron acceptor one.[7] In addition, these materials could prevent large-scale phase separation found in organic semiconductor blends by reaching thermodynamically stable nanostructures through microphase segregation. These cylindrical or lamellar morphologies oriented perpendicular to the electrodes could provide a path to obtain optimal exciton dissociation and

charge transport in active layer structures along with a long-term stability.[8] Different studies have shown the possibility to use them as a single component in active layer of solar cells with efficient records near 3%.[9, 10]

This is certainly low but it is related to the difficulty to synthesize such kind of materials, which makes the number of studied candidates quite reduced. Three strategies exist to produce all-conjugated diblock copolymers. The first one is based on the coupling of two macromolecules bearing functional groups at their end-chains, able to react with each other. The so-called "click chemistry" has been developed with this objective and the Huisgen cyclo-addition has been successfully used to create copolymers presenting interesting film morphologies.[11] The main difficulty with this route is to be able to reach a high overall yield because of the multiple steps and the non-complete functionalization of the parent homopolymers. The second strategy is the use of a sequential monomer addition in the polymerization batch.[12] Although this method shines by its simplicity, it implies full conversion of the first monomer before introducing the second one and limits the range of monomers to those polymerizable with the same coupling reaction. The third option is the "end-functional coupling method" that relies on the synthesis of a first block, bearing a functional group able either to initiate the chain polymerization of the second monomer[13] or to react as a monofunctional macromonomer in a step-growth polycondensation[14, 15]. This strategy is very interesting because it is only a two-step procedure allowing the combination of different polymerizations mechanisms which implies a large choice of monomers. Another important parameter is the choice of the linker between blocks. Lee *et al.* recently showed that the introduction of a flexible and non-conjugated spacer between two LBG blocks improved the PV performances by increasing the degree of crystallization of blocks.[16] Hu *et al.* studied block copolymers based on P3HT. On the contrary, they found out that the longer

the flexible spacer is the weaker the quenching is between donor and acceptor blocks. As a consequence decreased PV performances compared to an analog copolymer presenting a rigid linker were observed.[17, 18] They reported that the flexible spacer allowed the block to rotate to a non-planar orientation leading to a significant loss of overlap and as a consequence a reduction of charge separation and recombination rates.

In this work, we use of this "end-functional coupling method" to synthesize a novel CBP, poly(3-hexylthiophene)-*block*-poly(dithienosilole-diketopyrrolopyrrole) (P3HT-*b*-P(DTS-DPP) (Scheme 1). Synthetic features are exposed and discussed on the basis of Carothers polycondensation theory. The presence of diblock and triblock copolymers was investigated thanks to precise analysis of the size exclusion chromatography and nuclear magnetic resonance results. A range of block copolymer compositions was obtained by varying the P3HT block length and the monomer feed ratio. Spectrophotometry highlighted the absorption complementarity of the blocks and reflected the chromophores composition presenting a first absorption peak around 400 nm pertaining to the P3HT block and a second one around 800 nm attributed to the low band-gap sequence. Cyclic voltammetry allowed to determine that the LUMO of the P3HT was higher than the P(DTS-DPP) one, showing the possible donor-acceptor nature of the copolymer. Finally, the different copolymers were integrated in solar cells with or without $PC_{60}BM$ leading to a highest efficiency around 2%. The photovoltaic results are linked with the morphology and thermal behavior observed by atomic force microscopy and differential scanning calorimetry.

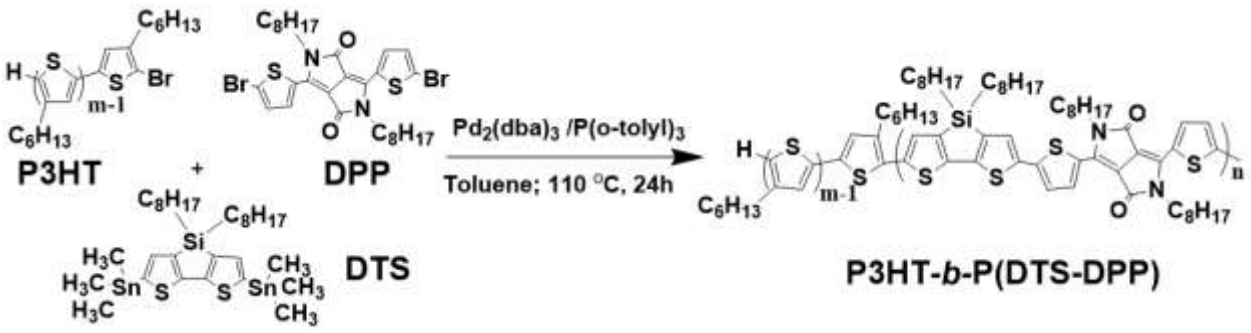

Scheme 1: Synthesis of fully conjugated diblock copolymer using Stille coupling of P3HT, DTS and DPP monomers.

2. Results and discussion

2.1. Synthesis of all-conjugated diblock copolymer

The synthesis of fully conjugated diblock copolymers was performed *via* subsequent Kumada catalyst transfer polymerization (KCTP) and Stille polycondensation. The first step was the synthesis of a brominated end-functional P3HT following the procedure developed by McCullough *et al.*[19] The procedure led to the elaboration of well-defined polymer with a molar mass of 13,000 g.mol^{-1} and a dispersity (Đ) around 1.7 (Figure SI-1), measured by size-exclusion chromatography (SEC). Since this mass is overestimated (because a conventional calibration from polystyrene standards was used), proton nuclear magnetic resonance (^{1}H NMR) was also performed. A degree of polymerization of 38 corresponding to an average number molar mass of 6,300 g.mol^{-1} (Figure SI-2, Table 1 entry 1) was obtained. Matrix assisted laser desorption ionization- time of flight (MALDI-TOF) analysis revealed that the polymer sample was composed of a mixture of 85 molar% of mono-brominated and 15% of α-ω-dibrominated chains. (Figure SI-3). This $P3HT_{38}$ was then used as a monobrominated end-capping agent in the Stille

polycondensation of a mixture of di-stannilated dithienosilole (DTS) with dibromodiketopyrrolopyrrole (DPP). The DPP monomer was synthesized and obtained with a yield higher than 76% and a high purity (97%) (see NMR spectrum in supporting information, Figure SI-4). The polymerization reaction was carried out in toluene at 110 °C for 24 hours using $Pd_2(dba)_3$/P(o-tolyl)$_3$ as the catalyst system (Scheme 1). The stoichiometry of monomers and end-capping agent in this reaction is a key factor that predetermines the length of the low band-gap block. In this paper, the stoichiometry of the species was maintained according to equation 1:

$$N_A = N_B + N_{B'} \quad \rightarrow \quad 2N_{DTS} = 2N_{DPP} + N_{P3HT} \qquad (1)$$

In which N_A, N_B, $N_{B'}$ represent the mole number of stannate functions and bromide groups pertaining to the DPP monomer and to the end-capping agent (P3HT), respectively. N_{DTS}, N_{DPP} and N_{P3HT} represent the number of DTS, DPP monomers and P3HT end-capper, respectively. By following this stoichiometry, the total number of aryl bromides is equal to the total number of aryl stannanes and the formation of chains containing P3HT is promoted. The number average degree of polymerization (DP_n) of polymers obtained in the case of A-A and B-B polycondensation, like DTS and DPP, with an end-capping agent, can be predicted thanks to Carothers equation (equation 2)[20, 21]:

$$\overline{DP_n} = \frac{1+r}{1+r-2rp} \qquad (2)$$

In which *r* is the ratio of monomer groups, and *p* is the conversion. It should be noted that in this equation, the calculated DP_n counts the number of DTS + DPP units, so it is twice the number of repeat units *n* used in the calculation of the number average molecular weight M_n. Therefore, M_n can be determined as follows (equation 3):

$$\bar{M}_n = M_0 \frac{\overline{DP_n}}{2} + xM_{P3HT} = \frac{M_0}{2}\frac{1+r}{1+r-2rp} + xM_{P3HT}$$

(3)

where M_0 and M_{P3HT} are the molecular weight of the repeat unit and end-group, respectively. x is the number of P3HT chains incorporated in the final material, and can be equal to 0, 1 or 2. When a monofonctional reagent (as the end-capping agent) is introduced, the monomer group ratio is defined by equation 4[20]:

$$r = \frac{N_A}{N_B + 2N_{B'}} = \frac{2N_{DTS}}{2N_{DPP} + 2N_{P3HT}} = \frac{N_{DTS}}{N_{DPP} + N_{P3HT}} \quad (4)$$

Where the factor 2, relative to $N_{B'}$, enters in the equation because the end-capping agent has the same effect on the degree of polymerization as the difunctional monomer therefore is two times more effective.

At the end of all polymerization reactions, the media were first precipitated in cold methanol and subsequently fractioned by Soxhlet extraction in acetone, cyclohexane and the polymer of interest was finally recovered from chloroform. The acetone and cyclohexane fractions were analyzed by UV-visible spectroscopy and size exclusion chromatography (Figure SI-5) and compared to pure P3HT and block copolymer final fractions. From these data it was easy to identify that acetone removed (i) unbound short P3HT chains, with an absorbance at 450 nm and a chromatogram peak corresponding to $P3HT_{38}$ homopolymer, and (ii) a small fraction of oligomers of P(DTS-DPP) with a secondary absorbance peak at 665 nm. Cyclohexane fraction was mainly constituted of P(DTS-DPP) low molar mass homopolymers, with a large SEC peak finishing after P3HT reference elution volume. Accordingly, the spectrophotometry of this sample showed no absorbance at 450 nm (*i.e.* no P3HT) and large absorbance band from 550 to

850 nm pertaining to the low band-gap sequence. The cyclohexane fraction contained low molar mass polymers, meaning that during the reaction, some DPP and DTS monomers reacted with each other but were not attached to a P3HT chain. For all synthesized block copolymers the percentage of removed homopolymer from acetone and cyclohexane Soxhlet extraction was around 10 w%. Another conclusion of this washing procedure removing homopolymers is that conversion is by definition below 1 for all copolymers synthesized.

A first block copolymer, reported in Table 1 entry 2, was synthesized from the $P3HT_{38}$ using DPP and DTS monomers with a feed molar composition of 1/0.98/0.04 equivalent of DTS/DPP/P3HT, satisfying equation 1. The final polymer, recovered from the chloroform Soxhlet fraction, was analyzed by SEC and Figure 1 shows the superposition of the pure $P3HT_{38}$ and the block copolymer $P3HT_{38}$-*b*-$P(DTS\text{-}DPP)_{19}$ using UV detector at two wavelengths; 450 nm to screen mainly the presence of the P3HT block and 720 nm to reveal the low band-gap block. Comparing both chromatograms registered at 450 nm, a clear shift towards the low retention volumes can be observed meaning an increase of the molar mass. The dispersity, measured by SEC increased from 1.7 to 3.4 because of the step-growth mechanism of the polycondensation. When the UV-detector was set to 720 nm, the chromatogram perfectly matches the one at 450 nm meaning that the low band-gap block has the same retention time as the P3HT block, proving their attachment.

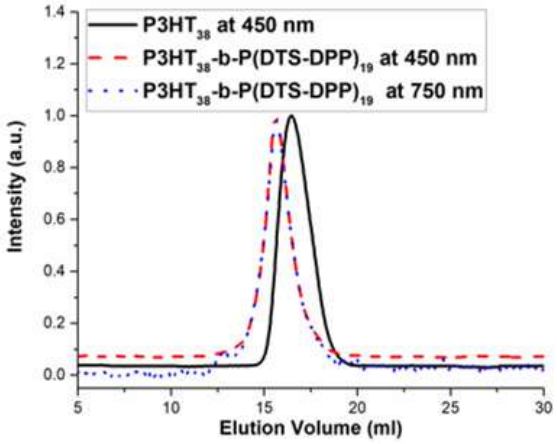

Figure 1: Size exclusion chromatograms using UV detector at 450 and 720 nm of the synthesized P3HT$_{38}$-*b*-P(DTS-DPP)$_{19}$ in comparison with the starting P3HT$_{38}$-Br at 450 nm.

The molar masses *Mn* obtained by SEC were 13,000 for the P3HT and 26,000 g.mol^{-1} for the copolymer (calculated from conventional calibration using polystyrene samples). To obtain more accurate values, ^{1}H NMR was performed to estimate the ratio between the P(DTS-DPP) repetitive unit and the P3HT end-chain ($N_{DTS\text{-}DPP}/N_{P3HT}$). Figure 2 shows the spectrum of P3HT$_{38}$-*b*-P(DTS-DPP)$_{19}$ in $C_2D_2Cl_4$. The comparison of the signal integral at 2.9 ppm pertaining to the CH_2 proton in alpha of the thiophene cycle of P3HT (2 protons *per* monomer unit) with the one at 4.2 ppm attributed to the CH_2 in alpha of the nitrogen in the DPP alkyl chains (4 protons *per* monomer unit) allowed to calculate a $N_{DTS\text{-}DPP}/N_{P3HT}$ ratio of 19 (Table 1 entry 2).

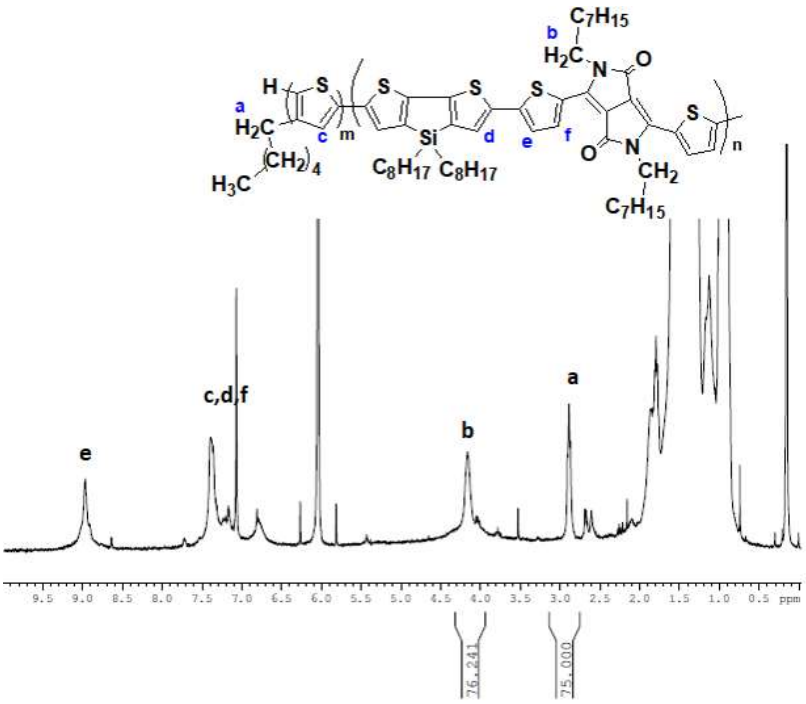

Figure 2: ^{1}H NMR spectrum of the synthesized $P3HT_{38}$-*b*-$P(DTS\text{-}DPP)_{19}$ ($C_2D_2Cl_4$, 400MHz).

Following the Carothers equation (2), at 100% conversion, the theoretical DP_n of the low band-gap block should be 100, corresponding to 50 DTS-DPP repetitive units. Since P3HT has been included in the stoichiometry, P3HT chains should be present at both ends of the low band-gap macromolecules (at 100% conversion) to produce a triblock. Therefore, for this theoretical polymer, the $N_{DTS\text{-}DPP}/N_{P3HT}$ ratio is 50/2 or 25 (reported in Table 1). The difference between the theory and the experiment (25 to 19) was low and due to the incomplete conversion, since unbound homopolymers have been found and extracted from the copolymer by Soxhlet extraction. Now, with an incomplete conversion, there may be a mixture of diblock $P3HT_{38}$-*b*-$P(DTS\text{-}DPP)_{19}$ and triblock $P3HT_{38}$-*b*-$P(DTS\text{-}DPP)_{38}$-*b*-$P3HT_{38}$ copolymers. Since the dispersity of the copolymer is high, chromatograms could not completely rule out the presence of triblock even though no shoulder in the high molar masses was detected.

Diffusion ordered spectroscopy (DOSY) NMR was used for to determine the diffusion coefficient of the species in the copolymer sample. The DOSY spectrum showed that only one diffusion coefficient could be detected with all the protons pertaining to the P3HT (at δ = 3 and 7 ppm) and the P(DTS-DPP) (at δ = 9 and 7.5 ppm) blocks aligned (see Figure SI-6). This is a clear indication that only one kind of macromolecules has been synthesized, and since the conversion is incomplete, the formation of triblock is excluded. Therefore, in Table 1, the degree of polymerization and molar masses were calculated from the ^{1}H NMR $N_{DTS\text{-}DPP}/N_{P3HT}$ ratio, by considering formation of diblock copolymers. The different synthesized samples were named in this report from these DP_n values.

Table 1: Molecular Characteristics for the synthesized block copolymers.

Entry	Polymer	N^a *DTS*	N^a *DPP*	N^a P3HT	$N_{DTS\text{-}DPP}/N_{P3HT}$ th[b]	DP_n P3HT-DP_n A-B[c]	*Mn* th[b] g.mol^{-1}	*Mn* exp[c] g.mol^{-1}	*Mn*[d] g.mol^{-1}	*Đ*[d]
1	$P3HT_{38}$	-	-	-	-	38-0	-	6,300	13,000	1.7
2	$P3HT_{38}$-*b*-$P(DTS\text{-}DPP)_{19}$	1	0.98	0.04	25	38-19	25,000	20,500	26,000	3.1
3	$P3HT_{38}$-*b*-$P(DTS\text{-}DPP)_4$	1	0.92	0.16	6	38-4	10,800	9,300	24,000	7.3
4	$P3HT_{240}$	-	-	-	-	240[e]-0	40,000[e]	-	19,000	2.1
5	$P3HT_{240}$-*b*-$P(DTS\text{-}DPP)_{10}$	1	0.98	0.04	25	240-10	58,000	48,000	26,700	2.1
6	P(DTS-DPP)	1	1	0	-	-	infinite	-	22,700	4.3

[a] feed ratio calculated according to equation 1, [b] calculated from Carothers equation with p = 1, [c] based on ^{1}H NMR, [d] measured by SEC and using a PS calibration, [e] this P3HT was commercially provided with a Mn = 40 000g.mol^{-1}.

Following the same procedure, a copolymer was synthesized from 0.16 eq of $P3HT_{38}$ for 1 eq of DTS and 0.92 of DPP, named $P3HT_{38}$-*b*-$P(DTS\text{-}DPP)_4$ (Table 1 entry 3). According to the

Carothers equation (2), a DP_n of 26 should be found at complete conversion, *i.e.* $N_{DTS\text{-}DPP}/N_{P3HT}$ ratio is 6. The purified polymer was characterized by ^{1}H NMR (Figure SI-7) and the experimental $N_{DTS\text{-}DPP}/N_{P3HT}$ was 4, in close agreement with the theoretical one. The molar mass *Mn* calculated from this value was 9,300 g.mol^{-1}. This time, size exclusion chromatography showed (Figure SI-8), in addition to the shift of the P3HT signal due to the formation of the diblock copolymer (elution volume of 16 mL), a shoulder corresponding to higher molar masses (elution volume of 13 mL) probably due to the presence of a non-negligible fraction of triblock copolymer. Since the equivalent of P3HT macromonomers was 4 times higher than in the first polymerization, the consumption of P3HT monofunctional reagent must also be higher leading to the formation of a certain amount of $P3HT_{38}$-*b*-$P(DTS\text{-}DPP)_8$-*b*-$P3HT_{38}$. As a consequence of this blend of copolymers, the dispersity of the sample was quite high, Đ = 7.3.

A third block copolymer was synthesized from a commercial P3HT with a high molar mass (40,000 g.mol^{-1}, Table 1 entry 4) commonly used to prepare solar cells with fair conversion efficiencies around 3.5%.[22] The commercial P3HT, bearing a bromide end-terminal group, was introduced as a monofunctional reagent (0.04 eq) in the Stille copolymerization (Table 1 entry 5) with DTS (1 eq) and DPP (0.98 eq). *^{1}H* NMR spectra of the commercial P3HT and the copolymer were performed and the $N_{DTS\text{-}DPP}/N_{P3HT}$ ratio was calculated to be 10 (Figures SI-9 and 10). This is lower than the expected value of 25 but can be explained by the high molar mass of P3HT, making it difficult the coupling to the low band-gap sequences. This agrees the SEC analysis (Figure SI-11) in which no shoulder pertaining to a hypothetic triblock was observed. The only shift from the P3HT reagent to the high molar mass was attributed to the elaboration of a diblock copolymer as discussed before. Finally, a control sample, P(DTS-DPP) (Table 1 entry 6) was synthesized in the absence of P3HT end-capping agent for the comparison with the block

copolymers in terms of optical and electronic properties, in which the results are discussed below.

2.2. Optoelectronic properties of the copolymers

The synthesized block copolymers were dissolved in chloroform and analyzed by UV-vis spectrophotometry. For $P3HT_n$-*b*-$P(DTS\text{-}DPP)_m$ copolymer, the spectra in Figure 3 showed two broad absorption bands. The first one with a λ_{max} of 445 nm is mainly attributed to P3HT absorption but also in a lesser extent to the P(DTS-DPP) block. Indeed, the spectra of P(DTS-DPP) homopolymer (Figure 3 green dashed dot line) shows a small absorption peak at 450 nm attributed to the π–π^* transition. It also exhibits a wide absorption band from 550 to 900 nm corresponding to the charge transfer interaction with two peaks at 745 and 800 nm. The vibronic shoulder at 800 nm suggests a strong interchain interaction in chloroform. The comparison of the $P3HT_n$-*b*-$P(DTS\text{-}DPP)_m$ spectra reflects the chromophore composition of the copolymers. Indeed, the absorbance ratio at λ = 445 nm and λ = 800 nm, A_{445}/A_{800}, is higher for the $P3HT_{240}$-*b*-$P(DTS\text{-}DPP)_{10}$ than $P3HT_{38}$-*b*-$P(DTS\text{-}DPP)_4$ and finally for $P3HT_{38}$-*b*-$P(DTS\text{-}DPP)_{19}$, 1.89, 1.02 and 0.33 respectively, in agreement with the block composition. Two optical band-gaps were calculated from the onset of the absorption wavelength at 550 and 920 nm for all copolymers with a value of 2.2 and 1.3 eV, respectively (Table 2).

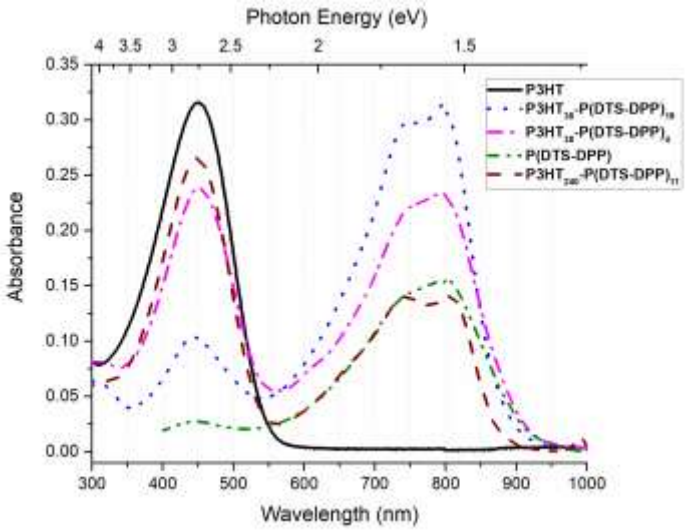

Figure 3: Spectrophotometry results of the synthesized homopolymers and copolymers made with DPP, DTS and P3HT in chloroform solutions.

The electrochemical properties of the synthesized conjugated block copolymers were determined by cyclic voltammetry. Polymer solutions in chloroform were prepared and deposited on a platinum working electrode by drop casting. The measurements allowed the detection of the oxidation and reduction potentials of the materials and therefore their HOMO and LUMO orbital levels. After measuring the oxidation/reduction of homopolymers P3HT and P(DTS-DPP), it was then possible to deduce the oxidation/reduction waves pertaining to each block of the conjugated copolymer (Figure SI-12). The values of the HOMO and LUMO levels of the polymers are summarized in Table 2. In the case of $P3HT_{38}$-*b*-$P(DTS\text{-}DPP)_{19}$ and $P3HT_{38}$-*b*-$P(DTS\text{-}DPP)_4$, two close oxidation states were identified in the voltammograms of the conjugated block copolymers, at -5.3 and -5.4 eV attributed to the P3HT and the low band-gap blocks, respectively. The copolymer voltammograms presented also two reduction waves at -3.8 and -2.9 eV pertaining to the P(DTS-DPP) and P3HT blocks, respectively. This result showed that a

donor-acceptor electron transfer is possible since the P3HT LUMO is higher than the P(DTS-DPP) one.

Table 2: Energy levels and band gaps of polymer thin films (eV).

Polymer	**E_{HOMO}** P3HT	**E_{LUMO}** P3HT	**E_{HOMO}** P(DTS-DPP)	**E_{LUMO}** P(DTS-DPP)	**Eg** [a] P3HT/P(DTS-DPP)	**Opt Eg** [b] P3HT/P(DTS-DPP)
$P3HT_{38}$	-5.3	-2.9	-	-	2.4/-	2.2
$P3HT_{240}$	-5.3	-2.9	-	-	2.4/-	2.1
P(DTS-DPP)	-	-	-5.7	-3.9	-/1.8	2.2/1.3
$P3HT_{38}$-*b*-$P(DTS\text{-}DPP)_{19}$	-5.3	-2.9	-5.4	-3.8	2.4/1.6	2.2/1.4
$P3HT_{38}$-*b*-$P(DTS\text{-}DPP)_{4}$	-5.3	-2.9	-5.4	-3.8	2.4/1.6	2.2/1.3
$P3HT_{240}$-*b*-$P(DTS\text{-}DPP)_{10}$	-5.3	-3.0	-5.6	-3.9	2.3/1.7	2.2/1.3

[a] measured by cyclic voltammetry and [b] measured by UV-vis spectrophotometry

2.3. Integration in solar cells

Thermal stability is an important parameter for the organic materials that will be used in optoelectronic applications. Thus, thermal gravimetric analysis (TGA) was conducted to investigate the thermal stability of the synthesized diblock copolymers. In all cases, a one-stage degradation was observed, starting around 400 °C with a residual mass of 50% (Figure SI-13). Thus, a safe thermal annealing of the active layer up to 200 °C is possible in all cases.

Solar cells with an inverted device architecture of ITO/ZnO/PEIE/photoactive layer/MoO_3/Ag were fabricated (Figure 4a). $P3HT_{38}$-*b*-$P(DTS\text{-}DPP)_4$ copolymer was used as a single component in the active layer given its donor-*b*-acceptor structure and the compatible HOMO-LUMO levels

measured by cyclic voltammetry. However, in this configuration, the efficiency was very low (almost zero) as shown in Table 3 entry 1. This could be explained by either a weak charge transfer between the P3HT block and the P(DTS-DPP) block and/or low electron and hole mobilities on the block copolymer layer. Photoluminescence spectroscopy was performed on this $P3HT_{38}$-*b*-$P(DTS\text{-}DPP)_4$ copolymer and compared with the P3HT homopolymer sample (Figure SI-14). A slight decrease of the photoluminescence intensity (~28% decrease) was observed in the copolymer sample compared to the homopolymer. Although electron transfer cannot be fully discarded, it is unlikely to be the main mechanism explaining this decrease. Indeed, this slight difference was rather assigned to (i) the slightly lower absorption of the copolymer sample at the excitation wavelength of 450 nm and (ii) the probable reabsorption of the P3HT emission from 550 to 650 nm by the P(DTS-DPP) block.

Thus, as electron transfer is not efficient between the two blocks of the copolymers, [6,6]-phenyl-C60-butyric acid methyl ester ($PC_{60}BM$) was added to the active layer in order to enhance the exciton dissociation and electron mobility without perturbing the complementary absorption of the copolymer. Thus, HOMO-LUMO levels of the PCBM used were also determined by cyclic voltammetry under the same condition as for polymers. The energy levels of the component materials are shown in Figure 4b.[23] Such an energy band alignment is expected to lead to an efficient charge separation of the generated excitons at the donor-acceptor interfaces.

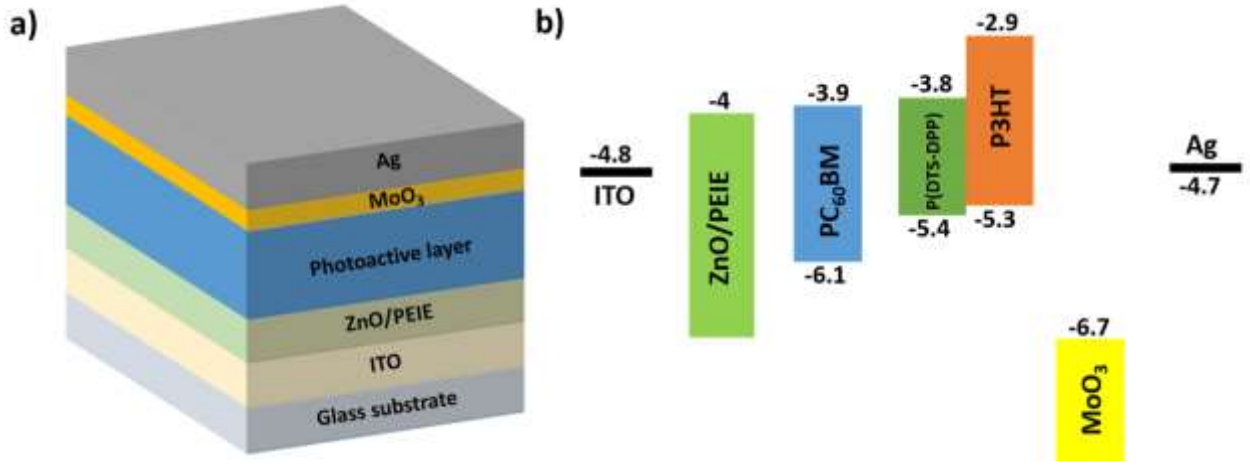

Figure 4: a) The fabricated inverted device architecture and b) energy levels (in eV) of the component materials used in such devices.

The active layers were first spin-coated from chlorobenzene solutions with a polymer:$PC_{60}BM$ mass ratio of 1:1 and a total concentration of 20 $mg.mL^{-1}$ (thickness ranging from 120 to 140 nm). The annealing temperature of the active layer was studied (annealing time of 10 minutes). Without annealing, the solar power conversion efficiency was 0.29%. By increasing the annealing temperature up to 120 °C, the efficiency was increased from 0.29 to 1.38% with an improvement in the short circuit current density (Jsc) from 1.51 to 6.71 mA/cm^2. This enhancement can be related to an improvement of the morphology and phase separation which increases the exciton dissociation rate and/or lead to the formation of collection pathways for the separated charges (see Figure SI-15 in supporting information). The crystallinity of the P3HT chains is also increased upon annealing, improving the hole mobility.[24] Above 120 °C, the drop in performance may be explained by the formation of large $PC_{60}BM$ clusters as previously described in the litterature.[25, 26] The donor:acceptor ratio was changed for 1:1.5 and 1:2 but the efficiency decreased to 1.24 and 1.10%, respectively with a drop in the short circuit current density (Table SI-1 in supporting information). This may be due to the P3HT crystallization

impeded by the fullerene molecules. This was observed in the absorption spectra of the blend active layer (Figure SI-16) in which the absorption band of P3HT (around 500 nm) undergoes a hypsochromic shift with an increasing amount of fullerene. It can also be noted that the absorption of the low band-gap block is weakly affected by the incorporation of $PC_{60}BM$. This may suggest that $PC_{60}BM$ has a stronger affinity for the P3HT block than for the P(DTS-DPP) one.

Table 3: Performances of solar cells integrating the synthesized copolymers.

Polymer	**Polymer: $PC_{60}BM$[a]**	**Annealing Temp (°C)**	**Solvent**	**FF**	**Voc (V)**	**Jsc (mA/cm^2)**	**PCE (%)**
	1:0	--------	Chlorobenzene	0.27	0.29	0.01	≈0
	1:1	--------	Chlorobenzene	0.31	0.63	1.51	0.29
	1:1	80	Chlorobenzene	0.38	0.43	4.76	0.78
$P3HT_{38}$-*b*-$P(DTS\text{-}DPP)_4$	1:1	120	Chlorobenzene	0.48	0.43	6.71	1.38
	1:1	150	Chlorobenzene	0.44	0.38	6.30	1.05
	1:1	120	Chloroform	0.37	0.36	0.9	0.12
	1:1	120	o-xylene	0.53	0.45	6.70	1.59
$P3HT_{240}$-*b*-$P(DTS\text{-}DPP)_{10}$	1:1	150	o-xylene	0.52	0.59	6.3	1.93
P3HT	1:1	120	o-xylene	0.48	0.6	6.6	1.90

[a] mass ratio

Given that the morphology has such an important impact on PV performances, the solvent of the donor:acceptor solution was changed from chlorobenzene to o-xylene and chloroform. The use of o-xylene significantly enhanced the PCE to 1.59%, by increasing both Jsc and open-circuit voltage (Voc) to 6.70 mA/cm^2 and 0.45 V, respectively with a FF of 53%. Moreover, this substitution has another benefit, as o-xylene is a non-chlorinated and less toxic solvent, commonly used by OPV industry. On the contrary, the use of chloroform leads to a strong decrease of the efficiency. The reason beyond this behavior could be the higher boiling point of o-xylene that stays a longer time than chlorobenzene and chloroform in the thin film before drying, giving more mobility to materials to self-organize.[27] This generally leads to a better phase-separation between the polymer and $PC_{60}BM$ with the formation of a bicontinuous network, thus increasing charge transport.[28] Although it is known that the addition of co-solvents may improve device performance by enhancing polymer crystallinity.[29] However, the incorporation of 3 w% additives such as diphenyl ether or acetophenone did not improve the efficiency (see Table SI-1 in the supporting information). Although efficiencies were increased by different optimization, they remained low for this block copolymer with a particularly low Voc (below 0.5 V).

The diblock copolymer with the highest molar mass (40,000 $g.mol^{-1}$), $P3HT_{240}$-*b*-$P(DTS\text{-}DPP)_{10}$, was then used as the donor material with the idea to enhance the crystallization and increase charges mobility. Organic solar cells based on $P3HT_{240}$-*b*-$P(DTS\text{-}DPP)_{10}$: $PC_{60}BM$ (mass ratio 1:1) were fabricated. The devices showed a PCE of 1.93% with Jsc of 6.3 mA/cm^2, Voc of 0.59 V and a FF of 52%. The difference with devices made with $P3HT_{38}$-b-$P(DTS\text{-}DPP)_4$, was mainly due to an increase in Voc. Under the same processing conditions, P3HT:$PC_{60}BM$-based

reference cells were fabricated for comparison in which they show a PCE of 1.90% (Table 3 and Figure 5).

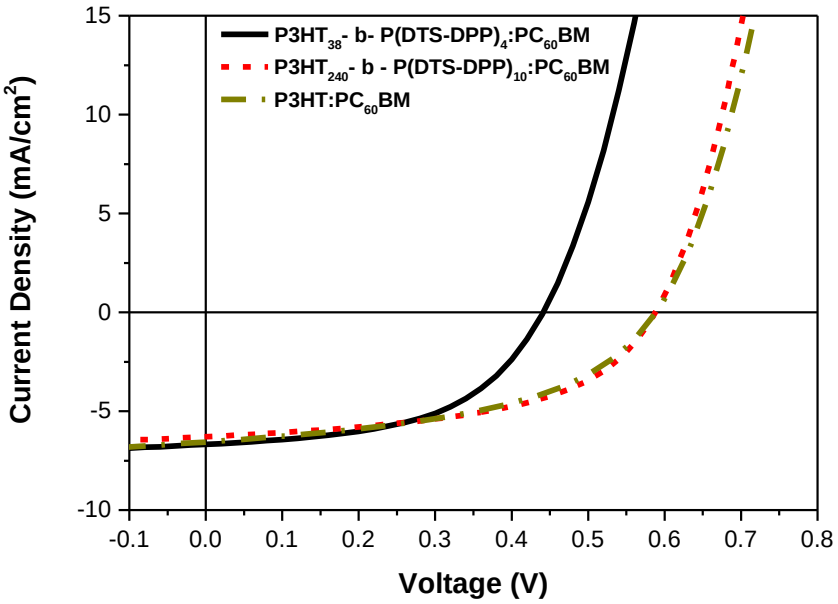

Figure 5: J-V curves of P3HT$_n$-*b*-P(DTS-DPP)$_m$:PC$_{60}$BM and P3HT:PC$_{60}$BM-based devices in o-xylene.

External quantum efficiency was measured for all devices. Results of the three best devices are plotted in Figure 6. For P3HT:PC$_{60}$BM-based devices, a maximum EQE of 40% was obtained at the typical maximum wavelength of P3HT, 500 nm. For P3HT$_{38}$-*b*-P(DTS-DPP)$_4$, a loss of EQE at 500 nm (to 32%) was balanced by the addition of the band, in the range 700 to 900 nm, due to the low band-gap block. This proves that charge dissociation occurs at the P(DTS-DPP):PC$_{60}$BM interface despite their low difference of LUMO energy. When P3HT$_{240}$-*b*-P(DTS-DPP)$_{10}$ was used, the EQE maximum at 500 nm was slightly higher (35%) and the photogeneration of charges from 700 to 900 nm was slightly shifted to the near infrared region with an EQE of 12%.

The absorbance and EQE profiles were compared for P3HT$_{38}$-*b*-P(DTS-DPP)$_4$ and P3HT$_{240}$-*b*-P(DTS-DPP)$_{10}$ in Figures SI-17 and SI-18, respectively. For both copolymers, the conversion of photons to electrons does not completely follows the absorbance spectrum, *i.e.* the contribution at 800 nm seems to be decreased. One can suggest that the long P3HT blocks lead to the formation of DTS-DPP clusters isolated in P3HT matrix. Such morphology would lower the interfaces between DTS-DPP and PC$_{60}$BM and hinder the dissociation of exciton formed in these isolated DTS-DPP areas. One can also notice that the difference between the LUMOs of P(DTS-DPP) and PC$_{60}$BM is lower than that of P3HT and PC$_{60}$BM. This could also reduce the electron transfer rate of the P(DTS-DPP) block.

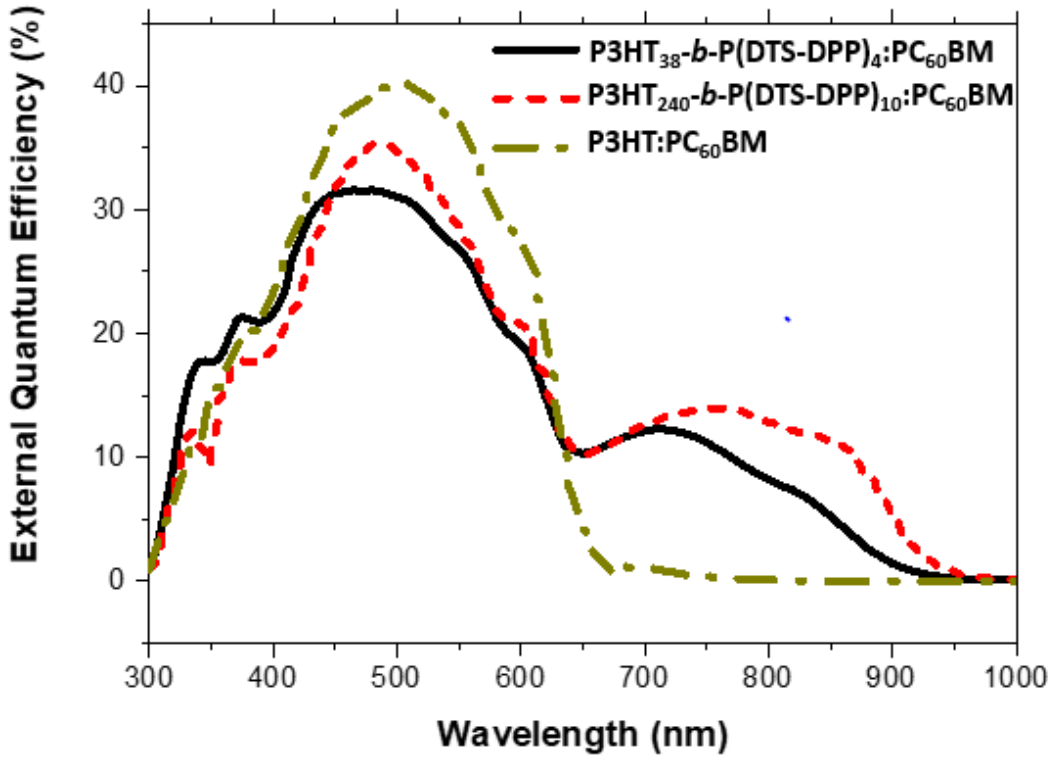

Figure 6. EQE spectra of P3HT$_n$-*b*-P(DTS-DPP)$_m$: PC$_{60}$BM and P3HT:PC$_{60}$BM-based solar cells.

Atomic Force Microscopy (AFM) was used to understand the variation in Voc and the decrease of EQE at 500 nm when the copolymers are used compared to P3HT homopolymer. The surface morphology of the photoactive layer, reported in Figure 7, showed a clear fibrillar structure for the P3HT blended with $PC_{60}BM$ (a,b). On the contrary, when $P3HT_n$-*b*-$P(DTS\text{-}DPP)_m$:$PC_{60}BM$ layers were analyzed, the nanomorphology appeared different. $P3HT_{38}$-*b*-$P(DTS\text{-}DPP)_4$:$PC_{60}BM$ (c,d) presents a nodular structure while $P3HT_{240}$-*b*-$P(DTS\text{-}DPP)_{10}$ (e,f) shows large clusters in comparison with P3HT:$PC_{60}BM$ active layer. These structural changes were also observed in pure polymer films (*i.e.* with no $PC_{60}BM$, see supporting information Figure SI-19). It has already been observed in previous studies that rod-*b*-rod block copolymers linked by a rigid unit, like thiophene in our case, could lead to a disruption of the crystallization of the individual blocks.[16, 18] On the one hand the nodular morphology and the intermixed organization could lead to an increase of non-geminate recombination as collection pathway are missing and this can explain the drop of Voc when $P3HT_{38}$-*b*-$P(DTS\text{-}DPP)_4$:$PC_{60}BM$ was used. In its turn, the high recombination in the active layer can explain the lower EQE values at 500 nm.[30] On the other hand, the high molar mass of P3HT and $P3HT_{240}$-*b*-$P(DTS\text{-}DPP)_{10}$, results in a fibrillar nanomorphology which improves Voc when compared to $P3HT_{38}$-*b*-$P(DTS\text{-}DPP)_4$:$PC_{60}BM$.[31] However, the larger clusters observed for $P3HT_{240}$-*b*-$P(DTS\text{-}DPP)_{10}$ can lead to geminate recombination which would decrease also the EQE. Therefore, in these copolymer systems, what is won with the photons absorbed in the 700 to 900 nm region and converted into electrons is lost with the copolymer structuration which lowers the number of charges collected at the electrodes.

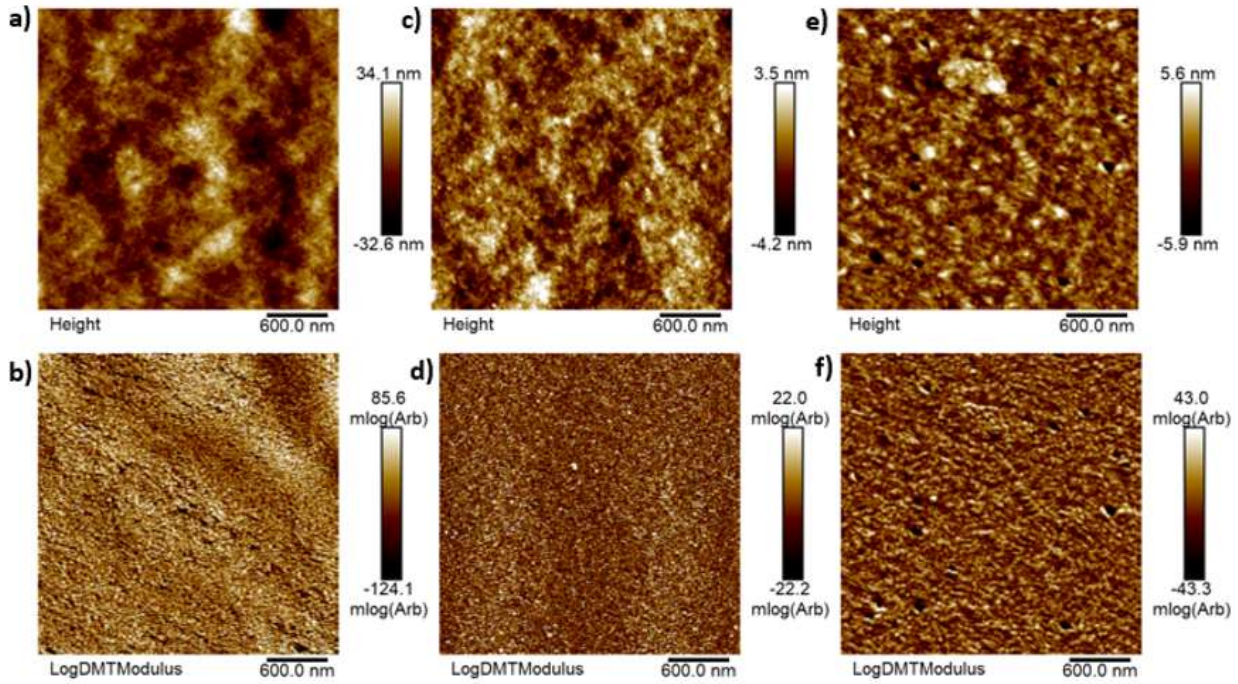

Figure 7. AFM images of a,b) P3HT:$PC_{60}BM$; c,d)$P3HT_{38}$-*b*-$P(DTS\text{-}DPP)_4$:$PC_{60}BM$ and e,f) $P3HT_{240}$-*b*-$P(DTS\text{-}DPP)_{10}$:$PC_{60}BM$ active layers.

$P3HT_{38}$-*b*-$P(DTS\text{-}DPP)_{19}$ was also used as the donor component in the active layer with $PC_{60}BM$ but conversion efficiencies were low, around 0.2%. Differential scanning calorimetry was used to emphasize the importance of P3HT crystallization in the copolymer (Figure SI-20). Before incorporation in diblock copolymers, P3HT homopolymers ($P3HT_{38}$ and $P3HT_{240}$) presented a sharp melting exotherm at 250 °C and a crystallization upon cooling at 200 °C. The analysis of the three diblock copolymers revealed that $P3HT_{38}$-*b*-$P(DTS\text{-}DPP)_{19}$ does not show any thermal transition, meaning an absence of melting and crystallization. This probably explains why this polymer is not itself an efficient donor in solar cells. On the contrary, the other two diblock copolymers presented a large melting temperature range at around 230 °C and a crystallization

peak at 170 °C. The shift of these values when compared with P3HT homopolymers illustrates a slight tendency of the P(DTS-DPP) block to impede the crystallization of the P3HT segments. This agrees with the AFM images shown in Figure 7 and SI-17.

3. Conclusion

Ternary blend, *i.e.* using DTS, DPP and P3HT monomers, were involved in Stille polymerization to produce block copolymers. In agreement with Carothers theory, the conversion *p* and monomer ratio *r* predetermined both the molar mass and the topology of the obtained macromolecules. Indeed, a low monofunctional reagent molar equivalent (N_{P3HT} = 0.04 eq) led to the synthesis of a diblock copolymer whereas a higher one (N_{P3HT} = 0.16 eq) generated a blend of diblock and triblock copolymers. Spectrophotometry revealed that the block molar composition was in agreement with the absorption profile, showing two complementary broad absorption bands in the 350-550 and 600-900 nm ranges assigned to the P3HT and the low band-gap blocks, respectively. Although the energy levels of the two blocks calculated from cyclic voltammetry could mean a donor-acceptor behavior, single components active layer solar cells presented very poor efficiency. Instead, the addition of $PC_{60}BM$ as an electron acceptor in the blend allowed the production of devices with efficiencies around 2% in which both the P3HT and low band-gap blocks contributed to the external quantum efficiency. The performances of the solar cells made from the copolymers were block composition dependent. In fact, long block of P(DTS-DPP) impeded the crystallization of P3HT and lowered the short circuit current. The best devices were obtained with the copolymer presenting the highest molar mass in which the morphology was optimized by the choice of a suitable solvent and thermal annealing.

4. Experimental section

4.1. Synthesis

Synthesis of P3HT-Br. P3HT were prepared by a Grignard metathesis polymerization as reported by McCullough *et al.*[19] The synthesis procedure is described in supporting information. Only the P3HT was provided by Solaris Chem with a Mn = 40 000g.mol^{-1} and a regioregularity of 94%.

Synthesis of diketopyrrolopyrrole monomer (DPP). DPP monomer was synthesized according to the synthetic route developed in literature by Naef *et al.* [32] The synthesis procedure is described in supporting information.

Synthesis of P(DTS-DPP). For the synthesis of P(DTS-DPP), all the materials were weighed in the glovebox, 1 eq of 4,4‘-Bis(2-ethyl-hexyl)-5,5'-bis(trimethyltin)-dithieno[3,2-b:2',3'-d]silole**,** DTS (120 mg, 0.16 mmol) was mixed under inert atmosphere in a microwave tube with 1 eq of DPP (110 mg, 0.16 mmol) in 2 mL anhydrous chlorobenzene. Tris(dibenzylideneacet-one) dipalladium(0) $Pd_2(dba)_3$ (6.00 mg, 0.0065 mmol) and tri(o-tolyl)phosphine P(o-tolyl)$_3$ ligand (8 mg, 0.026 mmol) were then added. The mixture was kept under inert atmosphere and stirred at 110 ^{o}C for 2 hours until the product become viscous. The polymer was precipitated in cold methanol and then filtrated. Soxhlet successive extractions were performed in acetone, methanol, and cyclohexane. The product was finally recovered in chloroform. The chloroform was then concentrated and the final dark black polymers P(DTS-DPP) was collected with a yield of 75 to 82%, dried under vacuum, then stored in the glovebox.

General procedure for the synthesis of P3HT$_n$-b-P(DTS-DPP)$_m$. The synthesis of all the studied P3HT$_n$-b-P(DTS-DPP)$_m$ was performed using the same procedure and under the same conditions. The main difference was only the ratio of the starting materials P3HT-Br and DPP

monomer. P3HT-Br was mixed in the glovebox with the di-stannylated DTS and di-brominated DPP monomers. $Pd_2(dba)_3$ catalyst (4 mg, 0.0043 mmol) and $P(o\text{-tolyl})_3$ ligand (5 mg, 0.016 mmol) were added to the reaction mixture. A flow of N_2 was applied for 15 minutes followed by the addition of 15 mL dry toluene. The mixture was bubbled with N_2 for 10 minutes before heating at 110 ^oC. After 24 hours, the mixture was cooled down and the crude conjugated block copolymer was precipitated in cold methanol and then filtrated. The obtained polymer was purified using a Soxhlet successive extractions in acetone, methanol, cyclohexane and finally collected in chloroform. The final polymer with yield of 70 to 85% was dried under vacuum and stored in the glovebox.

4.2. Characterization

Nuclear magnetic resonance (NMR) spectroscopy. Proton and diffusion ordered spectroscopy (DOSY) NMR spectra were recorded in deuterated tetrachloroethane as solvent using a Brüker 400 MHz spectrometer at 80 °C.

Size exclusion chromatographie (SEC) was performed using a bank of 4 columns (Shodex KF801, 802.5, 804 and 806) each 300 mm x 8 mm at 30 °C with THF eluent at a flow rate of 1.0 $ml.min^{-1}$ controlled by a Malvern pump (Viskotek, VE1122) and connected to Malvern VE3580 refractive index (RI) and Malvern VE3210 UV-visible detectors. Conventional calibration was performed against polystyrene standards.

Matrix assisted laser desorption ionization- time of flight. MALDI-MS spectra were performed by the CESAMO (Bordeaux, France) on a Voyager mass spectrometer (Applied Biosystems). The instrument was equipped with a pulsed N_2 laser (337 nm) and a time-delayed extracted ion source. Spectra were recorded in the positive-ion mode using the reflectron and

with an accelerating voltage of 20 kV. Samples were dissolved in THF at 10 mg/ml. The DCTB matrix -2-[3-(4-*t*-butylphenyl)-2-methyl-2-propenylidene]malononitrile solution was prepared at a concentration of 10 $mg.mL^{-1}$ in THF. The solutions were combined in a 10:1 volume ratio of matrix to sample. One to two microliters of the obtained solution were deposited to the sample target and vacuum-dried.

Absorption spectroscopy. The absorption spectra were recorded at room temperature with a double beam Cary 5000 spectrophotometer in steps of 1 nm in the range 400-1600 nm using a 1 cm quartz optical cell (Hellma).

Emission spectroscopy (photoluminescence). Corrected steady-state emission and excitation spectra were recorded at 1 nm resolution using a photon counting Edinburgh FLS920 fluorescence spectrometer with a xenon lamp. The concentrations in $CHCl_3$ were adjusted to an absorbance around 0.1 at 450 nm (excitation wavelength) in a 1 cm quartz fluorescence cell (Hellma).

Cyclic voltammetry (CV). A standard three-electrode electrochemical setup (AUTOLAB PGSTAT 101) consisting of a glassy carbon or a platinium disk as working electrode (2 mm diameter), a platinum foil as counter electrode, and a Ag/AgCl as reference electrode, was used in the electrochemical experiments. At the end of each experiment performed in CH_3CN/Bu_4NPF_6 (0.1 M), the standard potential of the ferrocenium/ferrocene couple, E_{Fe} , was measured, and all potentials were referenced against SCE using a previous determination of E_{Fe} = 0.41 V versus SCE in CH_3CN.(ref 1) Polymers were drop casted from a 10 mg/mL polymer solution in chlorobenzene/Bu_4NPF_6 (0,1 M) on the working electrode. CV gives direct information of the oxidation and reduction potentials of materials. The oxidation process corresponds to removal of the electron from the HOMO energy level, while the reduction

corresponds to electron addition to the LUMO energy level of the material. Therefore HOMO and LUMO energy levels can be estimated using the empirical equations: $E_{HOMO} = - (E_{ox} + 4.7)$ and $E_{LUMO} = - (E_{red} + 4.7)$, where E_{ox} and E_{red} are respectively the onset potentials for oxidation and reduction peaks relative to SCE and 4.7 the factor connecting SCE to vacuum [33]. The onset potentials are determined by the tangent method (see supporting information). Only values from the first sweep on a film were used as the film is changed or destroyed during the first oxidation. The scan rate used was 0.1 $V.s^{-1}$.

Thermal gravimetric analysis. TGA was performed on a TGA Q50, TA Instruments at a heating rate of 10 °C min^{-1} under nitrogen. *UV-visible absorption spectra* were recorded on a Shimadzu UV-2450PC spectrophotometer**.**

Differential scanning calorimetry. DSC experiments were performed using Q100 DSC from TA instruments under nitrogen atmosphere. For each sample, the temperature was increased from 40 to 240 °C with a ramp of 10 °C/min, then cooled to -65 °C at the same ramp. This was repeated during a second cycle.

Atomic force microscopy. A MultiMode® 8 Atomic Force Microscope (AFM) from Bruker was used in a PeakForce QNM (Quantitative NanoMechanics) mode.

4.3. Solar cell fabrication

The ITO substrates were pre-cleaned before use in which they were successively immersed in deionized water, acetone, ethanol and isopropanol with ultrasonication at room temperature. Then, they were dried and exposed to UV-O_3 cleaner chamber for 15 minutes at 80 °C in order to remove any residual organic contamination and to increase the hydrophilic nature of the surface. All the fabricated solar cells were based on the inverted device architecture. For their preparation

we proceed as follows: 0.15 mol.L^{-1} ZnO solution was prepared by mixing 66 mg zinc acetate in 2 mL absolute ethanol and 18 µL ethanolamine. The solution was stirred at 55 ^{o}C for 30 minutes before it was cooled down and spin coated on top of the pre-cleaned ITO substrates at 2000 RPM/1 minute. The layers were annealed at 195 °C for 30 minutes in air. PEIE solution (600 µL PEIE in 50 mL deionized water) was then spin coated on top of the ZnO layer at 5000 RPM/1 minute then annealed at 100 ^{o}C for 10 minutes in air. The substrates were then transferred into a nitrogen filled glovebox (O_2 < 1 ppm; H_2O < 1 ppm) to proceed with the photoactive layer deposition. The blend solutions were prepared and annealed at 70 ^{o}C overnight. The active layer was then deposited on top of the PEIE layer at 800 RPM/50 seconds followed by 1000 RPM/3 seconds. The layers were annealed at 120 °C for 10 minutes. Then, the substrates were placed into an evaporator inside the glovebox, in which a 10 nm-thick MoO_3 layer and a 70 nm-thick Ag anode layer were thermally evaporated at 8 × 10^{-6} Torr pressure through a shadow mask defining 10 mm^2 active area. The current density-voltage (J-V) characteristics of the cells were measured under N_2 using a K.H.S. SolarCelltest-575 solar simulator with HMI source and under illumination using an AM1.5 filters (ATLAS). The metal halide was set at 100 mW/cm^2 and using an IL1400BL calibrated radiometer.

ASSOCIATED CONTENT

Supporting Information

The supporting information provides synthetic scheme, chemical (SEC, NMR), thermal, optical, electronic, morphological, and photovoltaic characterization of the materials used in this study.

AUTHOR INFORMATION

Corresponding Authors

e-mail: antoine.bousquet@univ-pau.fr, christine.lartigau-dagron@univ-pau.fr

Funding Sources

ACKNOWLEDGMENT

The authors would like to acknowledge the National Council for Scientific Research of Lebanon (CNRS-L), Campus France and the Université de Pau et des Pays de l'Adour (UPPA) for the granting of Hisham Idriss, and UPPA for the granting of Adele Gapin. Abdel Khoukh and Virginie Pellerin are greatly thanked for their involvement in the project.

Reference

1. Ibn-Mohammed, T.; Koh, S. C. L.; Reaney, I. M.; Acquaye, A.; Schileo, G.; Mustapha, K. B.; Greenough, R. Perovskite solar cells: An integrated hybrid lifecycle assessment and review in comparison with other photovoltaic technologies. *Renewable and Sustainable Energy Reviews* **2017,** 80, 1321-1344.
2. Wadsworth, A.; Moser, M.; Marks, A.; Little, M. S.; Gasparini, N.; Brabec, C. J.; Baran, D.; McCulloch, I. Critical review of the molecular design progress in non-fullerene electron acceptors towards commercially viable organic solar cells. *Chemical Society Reviews* **2019,** 48 (6), 1596-1625.
3. Sommer, M.; Komber, H.; Huettner, S.; Mulherin, R.; Kohn, P.; Greenham, N. C.; Huck, W. T. S. Synthesis, Purification, and Characterization of Well-Defined All-Conjugated Diblock Copolymers PF8TBT-b-P3HT. *Macromolecules* **2012,** 45 (10), 4142-4151.
4. Wang, S.; Jin, X.; Yao, B.; Du, X.; Dong, L.; Wang, X.; Huang, W. Influence of the molecular weight in P3HT block on fully conjugated block copolymers. *Synthetic Metals* **2019,** 253, 20-25.
5. Woody, K. B.; Leever, B. J.; Durstock, M. F.; Collard, D. M. Synthesis and Characterization of Fully Conjugated Donor–Acceptor–Donor Triblock Copolymers. *Macromolecules* **2011,** 44 (12), 4690-4698.
6. Izuhara, D.; Swager, T. M. Poly(3-hexylthiophene)-block-poly(pyridinium phenylene)s: Block Polymers of p- and n-Type Semiconductors. *Macromolecules* **2011,** 44 (8), 2678-2684.
7. Wang, J.; Higashihara, T. Synthesis of all-conjugated donor-acceptor block copolymers and their application in all-polymer solar cells. *Polymer Chemistry* **2013,** 4 (22), 5518-5526.
8. Topham, P. D.; Parnell, A. J.; Hiorns, R. C. Block copolymer strategies for solar cell technology. *Journal of Polymer Science, Part B: Polymer Physics* **2011,** 49 (16), 1131-1156.
9. Miyanishi, S.; Zhang, Y.; Hashimoto, K.; Tajima, K. Controlled Synthesis of Fullerene-Attached Poly(3-alkylthiophene)-Based Copolymers for Rational Morphological Design in Polymer Photovoltaic Devices. *Macromolecules* **2012,** 45 (16), 6424-6437.
10. Guo, C.; Lin, Y.-H.; Witman, M. D.; Smith, K. A.; Wang, C.; Hexemer, A.; Strzalka, J.; Gomez, E. D.; Verduzco, R. Conjugated Block Copolymer Photovoltaics with near 3% Efficiency through Microphase Separation. *Nano Letters* **2013,** 13 (6), 2957-2963.

11. Smith, K. A.; Lin, Y.-H.; Dement, D. B.; Strzalka, J.; Darling, S. B.; Pickel, D. L.; Verduzco, R. Synthesis and Crystallinity of Conjugated Block Copolymers Prepared by Click Chemistry. *Macromolecules* **2013,** 46 (7), 2636-2645.
12. Chan, S.-H.; Lai, C.-S.; Chen, H.-L.; Ting, C.; Chen, C.-P. Highly Efficient P3HT: C60 Solar Cell Free of Annealing Process. *Macromolecules* **2011,** 44 (22), 8886-8891.
13. Wang, J.; Ueda, M.; Higashihara, T. Synthesis of All-Conjugated Donor–Acceptor–Donor ABA-Type Triblock Copolymers via Kumada Catalyst-Transfer Polycondensation. *ACS Macro Letters* **2013,** 2 (6), 506-510.
14. Nakabayashi, K.; Mori, H. All-Polymer Solar Cells Based on Fully Conjugated Block Copolymers Composed of Poly(3-hexylthiophene) and Poly(naphthalene bisimide) Segments. *Macromolecules* **2012,** 45 (24), 9618-9625.
15. Ku, S.-Y.; Brady, M. A.; Treat, N. D.; Cochran, J. E.; Robb, M. J.; Kramer, E. J.; Chabinyc, M. L.; Hawker, C. J. A Modular Strategy for Fully Conjugated Donor–Acceptor Block Copolymers. *J. Am. Chem. Soc.* **2012,** 134 (38), 16040-16046.
16. Lee, D. H.; Lee, J. H.; Kim, H. J.; Choi, S.; Park, G. E.; Cho, M. J.; Choi, D. H. (D)n-σ-(A)m type partially conjugated block copolymer and its performance in single-component polymer solar cells. *Journal of Materials Chemistry A* **2017,** 5 (20), 9745-9751.
17. Mok, J. W.; Lin, Y. H.; Yager, K. G.; Mohite, A. D.; Nie, W.; Darling, S. B.; Lee, Y.; Gomez, E.; Gosztola, D.; Schaller, R. D.; Verduzco, R. Conjugated Polymers: Linking Group Influences Charge Separation and Recombination in All-Conjugated Block Copolymer Photovoltaics (Adv. Funct. Mater. 35/2015). *Adv. Funct. Mater.* **2015,** 25.
18. Hu, Z.; Jakowski, J.; Zheng, C.; Collison, C. J.; Strzalka, J.; Sumpter, B. G.; Verduzco, R. An experimental and computational study of donor–linker–acceptor block copolymers for organic photovoltaics. *J. Polym. Sci., Part B: Polym. Phys.* **2018,** 56 (16), 1135-1143.
19. Iovu, M. C.; Sheina, E. E.; Gil, R. R.; McCullough, R. D. Experimental Evidence for the Quasi-"Living" Nature of the Grignard Metathesis Method for the Synthesis of Regioregular Poly(3-alkylthiophenes). *Macromolecules* **2005,** 38 (21), 8649-8656.
20. Knoester, H. Theoretical Derivation of the Molecular Weight Distribution of End-Capped Linear Condensation Polymers. *Macromol. Theory Simul.* **2009,** 18 (1), 61-69.
21. Flory, P. J. Molecular Size Distribution in Linear Condensation Polymers1. *J. Am. Chem. Soc.* **1936,** 58 (10), 1877-1885.
22. Dang, M. T.; Hirsch, L.; Wantz, G. P3HT:PCBM, Best Seller in Polymer Photovoltaic Research. *Advanced Materials* **2011,** 23 (31), 3597-3602.
23. Kröger, M.; Hamwi, S.; Meyer, J.; Riedl, T.; Kowalsky, W.; Kahn, A. Role of the deep-lying electronic states of MoO3 in the enhancement of hole-injection in organic thin films. *Applied Physics Letters* **2009,** 95 (12), 123301.
24. Hiorns, R. C.; de Bettignies, R.; Leroy, J.; Bailly, S.; Firon, M.; Sentein, C.; Khoukh, A.; Preud'homme, H.; Dagron-Lartigau, C. High Molecular Weights, Polydispersities, and Annealing Temperatures in the Optimization of Bulk-Heterojunction Photovoltaic Cells Based on Poly(3-hexylthiophene) or Poly(3-butylthiophene). *Advanced Functional Materials* **2006,** 16 (17), 2263-2273.
25. Lu, Y.; Wang, Y.; Feng, Z.; Ning, Y.; Liu, X.; Lü, Y.; Hou, Y. Temperature-dependent morphology evolution of P3HT:PCBM blend solar cells during annealing processes. *Synthetic Metals* **2012,** 162 (23), 2039-2046.
26. Miyanishi, S.; Tajima, K.; Hashimoto, K. Morphological stabilization of polymer photovoltaic cells by using cross-linkable poly(3-(5-hexenyl)thiophene). *Macromolecules* **2009,** 42 (5), 1610-1618.
27. Dang, M. T.; Wantz, G.; Bejbouji, H.; Urien, M.; Dautel, O. J.; Vignau, L.; Hirsch, L. Polymeric solar cells based on P3HT:PCBM: Role of the casting solvent. *Solar Energy Materials and Solar Cells* **2011,** 95 (12), 3408-3418.

28. Shin, P.-K.; Kumar, P.; Kumar, A.; Kannappan, S.; Ochiai, S. Effects of Organic Solvents for Composite Active Layer of PCDTBT/PC₇₁BM on Characteristics of Organic Solar Cell Devices. *International Journal of Photoenergy* **2014,** 2014, 786468.
29. Fontana, M. T.; Kang, H.; Yee, P. Y.; Fan, Z.; Hawks, S. A.; Schelhas, L. T.; Subramaniyan, S.; Hwang, Y.-J.; Jenekhe, S. A.; Tolbert, S. H.; Schwartz, B. J. Low-Vapor-Pressure Solvent Additives Function as Polymer Swelling Agents in Bulk Heterojunction Organic Photovoltaics. *The Journal of Physical Chemistry C* **2018,** 122 (29), 16574-16588.
30. Kline, R. J.; McGehee, M. D.; Kadnikova, E. N.; Liu, J.; Fréchet, J. M. J.; Toney, M. F. Dependence of Regioregular Poly(3-hexylthiophene) Film Morphology and Field-Effect Mobility on Molecular Weight. *Macromolecules* **2005,** 38 (8), 3312-3319.
31. Yu, J.; Tang, J.; Wang, C.; Zheng, Y.; Adachi, C.; Zeng, C. In *Influence of P3HT molecular weight on film processing and solar cell performance*, Proceedings - 2018 19th International Conference on Electronic Packaging Technology, ICEPT 2018, 2018; 2018; pp 1602-1604.
32. Naef, R. Synthesis, 1H-NMR and electronic absorption spectra of 2,6-disubstituted derivatives of 2,6-dihydrobenz [1,2-c:4,5-c']dipyrazol-3,7-dione. *Dyes and Pigments* **1991,** 17 (2), 113-121.
33. Brédas, J. L.; Silbey, R.; Boudreaux, D. S.; Chance, R. R. Chain-length dependence of electronic and electrochemical properties of conjugated systems: Polyacetylene, polyphenylene, polythiophene, and polypyrrole. *J. Am. Chem. Soc.* **1983,** 105 (22), 6555-6559.